SECRET

MARTIN MARIETTA ENERGY SYSTEMS LIBRARIES
3 4456 0360337 6

ORNL 187
PHYSICS_FISSION

Copy 4/A

CENTRAL RESEARCH LIBRARY
DOCUMENT COLLECTION

PHYSICS DIVISION

FINAL REPORT

SLOWING DOWN OF FISSION NEUTRONS IN GRAPHITE

J.E. HILL
L.D. ROBERTS
G. McCAMMON

CENTRAL RESEARCH LIBRARY
DOCUMENT COLLECTION
LIBRARY LOAN COPY
DO NOT TRANSFER TO ANOTHER PERSON
If you wish someone else to see this document, send in name with document and the library will arrange a loan.

OAK RIDGE NATIONAL LABORATORY

OPERATED BY
CARBIDE AND CARBON CHEMICALS CORPORATION
FOR THE
ATOMIC ENERGY COMMISSION
POST OFFICE BOX P
OAK RIDGE, TENNESSEE

TRANSMITTAL DATED 1-20-49

SECRET

ORNL-187

[redacted]

DECLASSIFIED Per Letter Instructions Of AEC-5-29-52 Without Deletions

This document consists of 35 pages.
Copy 4 of 86, Series A.

ISSUED: 706-A Library

8-12-52

SUPERVISOR CENTRAL FILES
ORNL

Contract No. W-7405, eng. 26

FINAL REPORT

SLOWING DOWN OF FISSION NEUTRONS IN GRAPHITE

J. E. Hill
L. D. Roberts
G. McCammon

DATE ISSUED:
JAN 19 1948

OAK RIDGE NATIONAL LABORATORY
operated by
Carbide and Carbon Chemicals Corporation
for the
Atomic Energy Commission
Post Office Box P
Oak Ridge, Tennessee

RESTRICTED DATA
This document contains restricted data as defined in the Atomic Energy Act of 1946.

CAUTION
This document contains information affecting the National Defense of the United States.
Its transmission or the disclosure of its contents in any manner to an unauthorized person is prohibited and may result in severe criminal penalties under applicable Federal laws.

[redacted]

MARTIN MARIETTA ENERGY SYSTEMS LIBRARIES
3 4456 0360337 6

SLOWING DOWN OF FISSION NEUTRONS IN GRAPHITE

J. E. Hill
L. D. Roberts
G. McCammon

A B S T R A C T

$\overline{\tau}$, $\overline{\tau^2}$ and $\overline{\tau^3}$ have been measured for a plane fission source in graphite. The values $\overline{\tau} = 310.6\ cm^2$, $\overline{\tau^2} = 11.48 \times 10^4\ cm^4$, and $\overline{\tau^3} = 5.23 \times 10^7\ cm^6$ were obtained. The value of $\overline{\tau} = 310.6\ cm^2$ is lower than the previously accepted value of $317\ cm^2$. It seems likely that certain transport corrections may not have been applied to the data in the earlier work, and that the difference between the earlier value and our result is due to this.

[redacted]
This document contains restricted data as defined in the Atomic Energy Act of 1946.
[redacted]
CAUTION
This document contains information affecting the National defense of the U.S. Its transmission or the disclosure of its contents in any manner to an unauthorized person is prohibited and may result in severe criminal penalties under applicable Federal laws.

I. INTRODUCTION

The purpose of this work was, first, to measure in graphite the spatial distribution of indium resonance neutrons from a fission source out to larger distances from the source than previous measurements had been carried; second, to see whether this extension of the measurements would affect the value of $\overline{z^2}$ now in use; and, third, to obtain $\overline{z^4}$ and higher moments if possible.

Previous measurements have used a point source of fission neutrons. In our experiments, to obtain a greater source strength, a plane source geometry was used. The theoretical treatment of Weinberg and Rose, MonP-240 and MonP-297, was used to reduce our moments measured in a finite graphite block to the corresponding moments for a (point) source in an infinite graphite block. (Thus, a fourth purpose of this work was to obtain an experimental check of this theoretical technique.)

II. EXPERIMENTAL DETAILS

(A) Introduction

The fission neutrons for the measurements were obtained by the capture of thermal neutrons in a U^{235} source mounted in a graphite prism. The thermal neutrons came from the thermal column of the ORNL pile. The spatial distribution in the graphite prism of indium resonance neutrons was measured by obtaining the saturated activity - A_s - on the source side of cadmium covered indium foils activated in the graphite

prism at various distances z, from the U^{235} source. The remainder of this section gives a detailed description of the experimental equipment, procedures and methods of analysis of data and results.

(B) Thermal Column of the ORNL Pile

This consisted of a stepped structure of graphite blocks which were very tightly stacked to obtain a high cadmium ratio and a symmetrical transverse flux distribution. The top surface of the column was 67-3/16" square. The thermal flux at the center of the column, position "A", Fig. 1, was about 10^6 neutrons/cm^2/sec. The indium resonance activity induced by the thermal column neutrons through 1/8" of cadmium, at this point and in the absence of the U^{235} source, was 1.5 β's/cm^2/sec, giving the rather high cadmium ratio of 140,000.

Since the old thermal column gave an asymmetric transverse distribution of thermal flux, a measurement of this transverse distribution was made at position "B", Fig. 1, and gave a $\cos \frac{\pi x}{a} \cos \frac{\pi y}{a}$ distribution to within 2%. This demonstrates the absence of any streaming of neutrons through cracks in the structure and also that there is no localized region of large absorption cross section due to impure graphite, etc.

(C) The Graphite Measurement Column

This was a prism of graphite 4' x 4' x 12', Fig. 1. It was constructed by stacking layers of graphite blocks, each block being 4' long by 4.00" x 4.00" in cross section. In stacking, the long dimension

Dr. 6300

FIG. 1

GRAPHITE MEASURING COLUMN

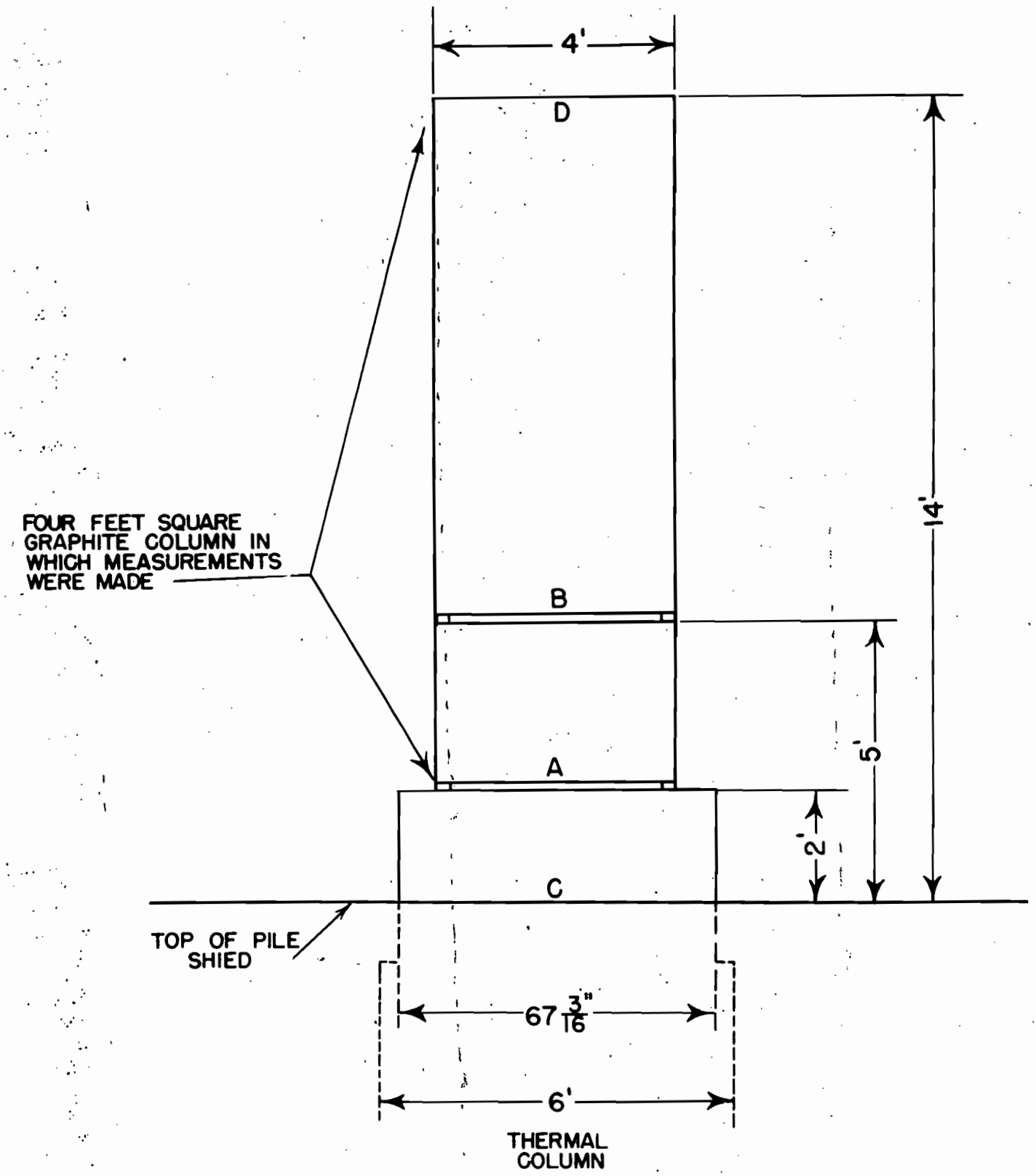

of the graphite blocks was alternated by 90° from layer to layer. Each block passing through the central vertical axis of the prism was removable, and was so cut that indium foils in their cadmium boxes could be placed at approximately 2" intervals up the central axis of the column all the way from "A" to "D", Fig. 1. Slots were provided at positions "A" and "B" which were 3/4" deep along z and approximately 4' x 4' in the transverse dimensions where the U^{235} source could be inserted into the column.

(D) Fast Neutron Source

The fast neutron source was made up from uranium which was 96% U^{235} alloyed with aluminum to form the eutectic alloy 18% in uranium by weight. This alloy was rolled to a sheet 0.040" thick and then cut into squares 4" on a side. Thirty-six of these squares were mounted on a graphite sheet in a checker board array as shown in Fig. 2. This sheet could be inserted into the graphite measurement column in the slots provided at either position "A" or "B", Fig. 1. When this sheet was in one position, the other position was filled by a plane graphite sheet (no uranium.)

As was pointed out above, the thermal flux at position "B", Fig. 1 was an almost perfect $\cos \frac{\pi x}{a} \cos \frac{\pi y}{a}$, where a is the effective transverse dimension of the sample. The fast neutron flux generated by this thermal flux would then have this same $\cos \frac{\pi x}{a} \cos \frac{\pi y}{a}$ distribution as its fundamental Fourier component. Due to the "checker board" character of the source, the fast neutron source distribution

SECRET

Dr. 6301

FIG. 2

U^{235} SOURCE ARRANGEMENT —

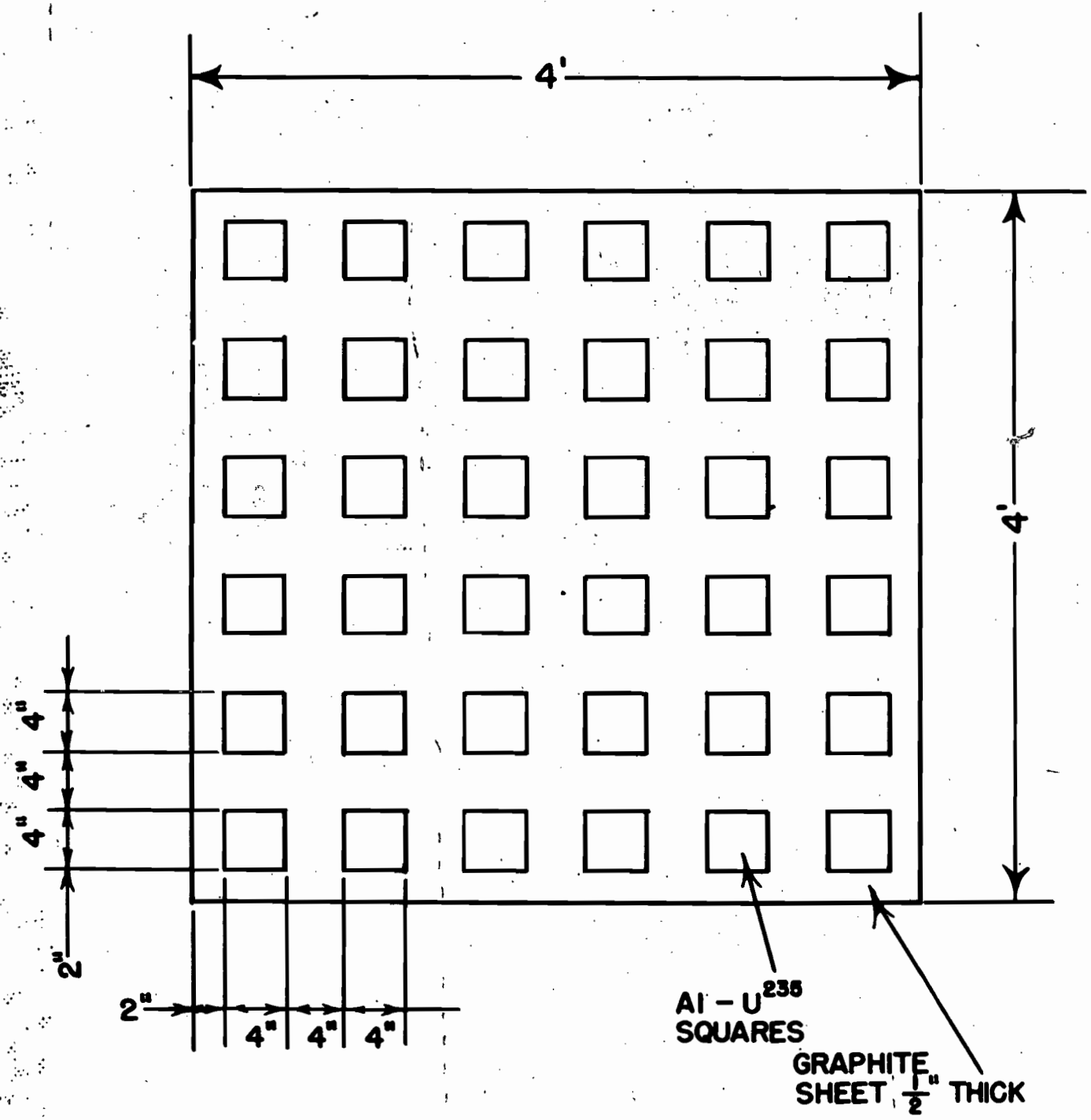

would have in addition certain higher Fourier components. The first two of these would be the 11th and 13th harmonics with amplitudes about equal to the amplitude of the fundamental. Age theory indicated that the amplitudes of these higher harmonics would be very violently damped relative to the fundamental component. This was found to be true. A measurement of the transverse indium resonance flux at position "B" gave a $\cos \frac{\pi x}{a} \cos \frac{\pi y}{a}$ to within 2%, the approximate error of the measurement. Thus, the checker board source was completely equivalent to a uniform plane sheet of uranium. This simple $\cos \frac{\pi x}{a} \cos \frac{\pi y}{a}$ was advantageous in the analysis of the results. A similar measurement just above the source in position "A" was not a simple cosine of wavelength 2a but contained higher harmonics due to the change in the column cross section from 67-3/16" to 48" at "A", Fig. 1. As will be seen later, these harmonics damp out so rapidly that there was no difference in the shape of the distribution, within experimental error, when the source was at position "A" or at position "B".

(E) Indium Foils and Cadmium Boxes

The indium foils used for all of the flux measurements were 4.00 cm. x 6.35 cm. in area and 93.8 mg/cm^2 thick (wt. 2.3825 g). New indium foils were used at the beginning of the series of measurements and a given foil was always used in the same position. This was done to maintain the smallest possible counter background relative to the flux to be

measured. For the measurement of the indium resonance flux, the foils were enclosed in cadmium boxes with a wall thickness of $\sim$ 0.135". When activating the indium foils in cadmium in the column, the foils were spaced about 10 cm. apart along z, and were parallel to the source plane. Two series of measurements were made, with the first foil 5 cm. from the source and with the first foil 10 cm. from the source, thus giving a measurement at every 5 cm. approximately. Measurements were made out to 118.7 cm. from the source, where the activity of the last foil was just twice the counter background. When possible, the foils were activated for at least two indium half lives and were counted for a total interval up to 28 minutes, depending on the foil activity. Each foil was counted on two counters. This gave a large total count and gave a constant check on counter and scaler operation.

(F) Data

Two experiments were made, first with the source in the upper position, "B", Fig. 1, and second, with the source in the lower position, "A", Fig. 1.

Upper Source Position.

The data taken with the source in this position are thought to be valuable because the graphite measurement column had the same transverse dimensions for a considerable distance above and below the source, and also the distribution of source energy neutrons was an almost perfect $\cos \frac{\pi x}{a} \cos \frac{\pi y}{a}$ (section D), these factors being important in the

analysis of the results. However, because of being relatively far from the pile, the source was relatively weak and measurements could be carried only out to 86 cm. The data for A_s vs. z are given in Table I.

TABLE I

SUMMARY OF EXPERIMENTAL DATA WITH SOURCE IN UPPER POSITION

Experiments No. 7, 8 12

z Distance in cm.	A_s Saturated Activity
4.80	22918
9.88	21446
14.96	18790
20.04	15803
25.12	12246
30.20	9469
35.28	6982
40.36	4978
45.44	3354
50.52	2274
55.60	1445
60.68	941
65.76	581
70.84	368
75.92	217
81.00	141
86.08	75

The data given are the average values of five experiments, the total count obtained on the points of low z being about 200,000, and for large z falling roughly in proportion to A_s to about 1,000. As will be discussed in the sections on theory and results, the use of these data for the calculation of $\overline{r^2}$ (average) around a point source in an

infinite medium requires the calculation of the $\overline{z^{2n}}$ average of data defined as

$$\overline{z^{2n}}(av) = \frac{\int_0^{\infty} A_s \, z^{2n} \, dz}{\int_0^{\infty} A_s \, dz}, \quad n = 0, 1, 2, 3, \ldots \qquad (1)$$

These integrals go from 0 to ∞ whereas the upper source position data go from 0 to 86 cm. only. It was assumed that an exponential integral extrapolation of the data would be suitable from 120 to ∞ giving

$$\overline{z^{2n}}(av) = \frac{\int_0^{120} A_s \, z^{2n} \, dz + K\int_{120}^{\infty} - E_i\left(-\frac{z}{\lambda}\right) z^{2n} \, dz}{\int_{\infty}^{120} A_s \, dz + K\int_{120}^{\infty} - E_i\left(-\frac{z}{\lambda}\right) dz} \qquad (2)$$

The first integral in the numerator and denominator of the above fraction was the area under the experimental points and the second integral was the calculated area of the exponential integral extrapolation.

Lower Source Position.

The data obtained with the source in the upper position were taken with the best conditions of geometry at the sacrifice of neutron source intensity. The source was then placed in position "A", Fig. 1 (lower source position) to obtain the largest possible source intensity at, what was first thought to be, a sacrifice of good geometry. However, as it turned out, the A_s vs. z curve taken

for the lower source position was strictly proportional to the entire 86 cm. of the A_s vs. z curve measured with the source in the upper position. Table II shows the data taken with the source in the lower position and Table III shows the strict proportionality of the two sets of data over the first 86 cm. range of z. Since the z positions were not identical in the two experiments, the A_s values for the experiment with the source in the upper position were read from the curve at the z values used in the experiment with the source in the lower position and are given in column 3 of Table III. Column 4 gives the ratio of the larger to the smaller activities for the same z values and column 5 the deviations of this ratio from the average value of 43.46. The maximum deviation is 3% with as many plus as minus. The r.m.s. deviation is 1.7% which is well within experimental error. Since the two curves are experimentally indistinguishable it was decided to average the two sets of data. This was done as follows. Since there were slight differences in the z values for the two positions (compare Tables I and II), a simple average of the z values was taken. For the corresponding A_s values, the points for the upper source position were multiplied by 43.46 and averaged with the points for the lower source position. Table IV gives the resulting values of z and A_s.

Since it is convenient in the analysis of the data to use numerical integration and differentiation methods which require equal intervals of z, values of Log_{10} (A_s) were plotted vs. z and a smooth curve

TABLE II

SUMMARY OF EXPERIMENTAL DATA WITH SOURCE IN THE LOWER POSITION

Experiments No. 13....19

z	A_s
4.94	1021226
10.02	916430
15.10	817790
20.18	670780
25.26	549748
30.34	409269
35.42	299752
40.50	217244
45.58	139973
50.66	95500
55.74	61536
60.82	40846
70.98	15415
81.14	5714
91.30	1986
98.38	1067
103.46	657
108.54	414
113.62	260
118.70	163

TABLE III

z	Lower Source Position (measured distribution)	Upper Source Position (read from curve of z values indicated)	Ratio	Deviation from Av ratio
4.94	1,021,000	22960	44.46	+ 1.00
10.02	916,400	21400	42.82	- 0.64
15.10	817,800	18720	43.69	+ .023
20.18	670,800	15560	43.11	- 0.34
25.26	549,700	12270	44.80	+ 1.34
30.34	409,300	9400	43.54	+ 0.08
35.42	299,800	6920	43.37	- 0.14
40.50	217,200	4904	44.29	+ 0.83
45.58	140,000	3310	42.30	- 1.16
50.66	95,500	2246	42.52	- 0.94
55.74	61,540	1425	43.19	- .27
60.82	40,850	935	43.69	+ 0.23
70.98	15,420	361	42.71	- .75
81.14	5,714	130	43.95	+ 0.49

TABLE IV

NORMALIZED DATA OF EXPERIMENTS NO. 7...19

z	A_s
4.87	1008500
10.02	924129
15.03	817108
20.11	678710
25.19	540918
30.27	410348
35.35	301560
40.43	216769
45.51	142852
50.59	97153
55.67	62161
60.75	40866
65.76	25244
70.91	15703
75.96	9429
81.07	5870
86.08	3256
91.30	1986
98.38	1067
103.46	657
108.54	414
113.62	260
118.70	163

fitted to the experimental points. Values of A_s were read from the curve at 2 cm. intervals from z = 0 to z = 120 cm. These results were checked by plotting a curve of $Log_{10}(A_s)$ vs. z^2 and reading the values of A_s at z^2 = 0, 4, 16, etc. The resulting values of A_s and z are given in Table V and graphs, on a reduced scale, of the curves mentioned above are shown in Fig. 3. The values of A_s at z = 0, 2 and 120 cm. were obtained by linear extrapolations on the $Log_{10}(A_s)$ vs. z^2 curve

TABLE V

SATURATED ACTIVITY AND LOGARITHM OF SATURATED ACTIVITY VERSUS DISTANCE AT 2 cm. INTERVALS TAKEN FROM GRAPH OF FIGURE III

z in cm.	A_s	$Log_{10}(A_s)$	z in cm.	A_s	$Log_{10}(A_s)$
0	1.0352×10^6	6.015	62	3.590×10^4	4.555
2	1.0257 "	6.011	64	2.993	4.476
4	1.0139 "	6.006	66	2.484	4.395
6	9.8860×10^5	5.995	68	2.061	4.314
8	9.6380 "	5.984	70	1.706	4.232
10	9.2900	5.968	72	1.406	4.148
12	8.9130	5.950	74	1.149×10^4	4.060
14	8.4340	5.926	76	9.333×10^3	3.970
16	7.9800	5.902	78	7.586×10^3	3.880
18	7.4140	5.870	80	6.166×10^3	3.790
20	6.8870	5.838	82	5.012 "	3.700
22	6.3100	5.800	84	4.074	3.610
24	5.7280	5.758	86	3.312	3.520
26	5.1880	5.715	88	2.717	3.434
28	4.6560	5.668	90	2.229	3.348
30	4.1690	5.620	92	1.841	3.265
32	3.6990	5.568	94	1.531	3.185
34	3.2810	5.516	96	1.277	3.106
36	2.8710×10^5	5.458	98	1.067×10^3	3.028
38	2.5360 "	5.404	100	8.913×10^2	2.950
40	2.2080	5.344	102	7.482 "	2.874
42	1.9060	5.280	104	6.238	2.795
44	1.6450	5.216	106	5.188	2.715
46	1.4060	5.148	108	4.326	2.636
48	1.1968	5.078	110	3.598	2.556
50	1.0186×10^5	5.008	112	3.006	2.478
52	8.610×10^4	4.935	114	2.501	2.398
54	7.312 "	4.864	116	2.085	2.319
56	6.110	4.786	118	1.738	2.240
58	5.129	4.710	120	1.446×10^2	2.160
60	4.306	4.634			

FIG. 3

SLOWING DOWN OF FISSION NEUTRONS IN GRAPHITE

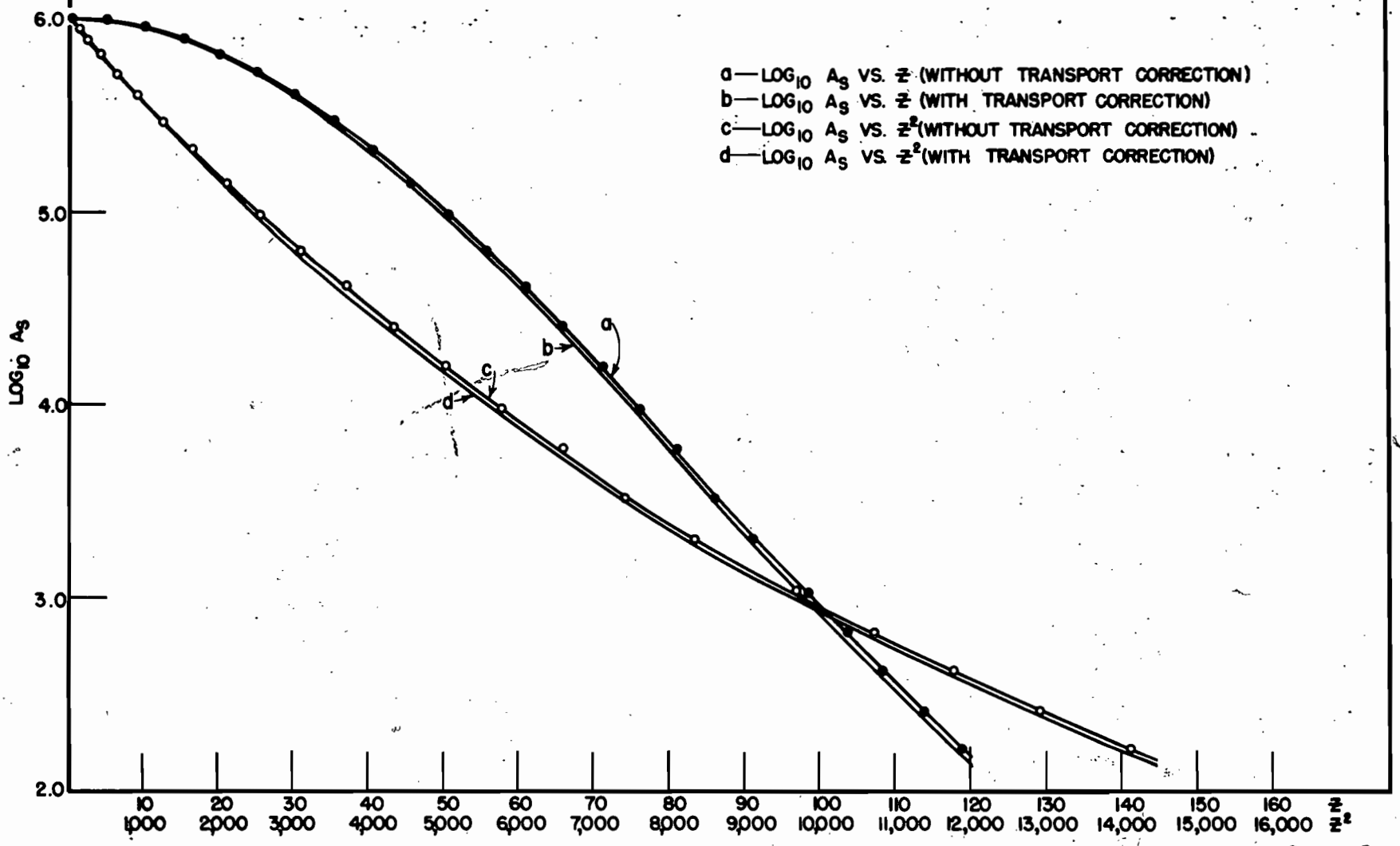

and are probably good within the experimental error since the distribution is nearly Gaussian for any given small interval of z.

(G) The Transport Correction

Since the measurements of A_s were always made by placing the source side of the foil next to the Geiger counter tubes the measured distribution given in Table V is not the true $A_s(z)$. The usual procedure is to measure the activities on both sides of the foil and take the average, i.e.

$$A_s(z) = \frac{A_{s\ front} + A_{s\ back}}{2} \tag{3}$$

This method is based on the following theoretical considerations. If one takes a solution to the Boltzmann equation which gives the flux in terms of an expansion in Legendre Polynomials and neglects all except the first two terms of the expansion, then

$$nv(z)_t = nv(z) + \lambda_t \left| \frac{d\left[nv(z)\right]}{dz} \right| \cos\theta \tag{4}$$

If this is integrated over the detecting foil, assuming that the foil is black to the indium resonance neutrons, that no neutrons entering from the back contribute to the activation of the source side and vice versa, that only activity from a given side is counted by the counter and that the self absorption of the radiation counted is the same for both sides of the detecting foils, then

$$A_{s\ front} = A_s(z) + \frac{\lambda_t}{2} \left| \frac{d\ A_s(z)}{dz} \right| \tag{5}$$

and similarly

$$A_{s\ back} = \qquad + \frac{\lambda_t}{2} \left| \frac{d\ A_s(z)}{dz} \right| \tag{6}$$

Solving (5) and (6) for $A_s(z)$ immediately gives (3) and it should be noted that (3) will be true for any constant coefficient of the derivative terms in (5) and (6) as long as the constant is the same in both (5) and (6). The authors have shown experimentally in making slowing down measurements on Sb-Be neutrons in the same sample of graphite that was used in this experiment, that

$$A_{s\ front} = A_s(z) + c \left| \frac{d\left(A_s\ z\right)}{dz} \right| \tag{7}$$

and

$$A_{s\ back} = A_s(z) - c \left| \frac{d\ A_s}{dz} \right| \tag{8}$$

The value of c obtained was 0.950 cm. which is less than $\frac{\lambda_t}{2}$ for graphite of 1.39 cm. This is not surprising, since the condition that only neutrons entering from the source side of the foil contribute to $A_{s(front)}$ and similarly for $A_{s(back)}$, which was used in deriving (5) and (6), is not fulfilled with foils of the thickness used in this experiment.

Since the same indium foils, Cd covers, counters and graphite sample were used in obtaining the distribution from the fission source as were used in the experiment described for determining c, it was convenient to correct the measured distribution of the activities, on the source side of the foils in this work, to the true distribution by the use of (7), which was done as follows:

Since

$$\frac{d\,A_s(z)}{dz} = 2.303\,A_s(z)\,\frac{d\left[\log_{10} A_s(z)\right]}{dz} \tag{9}$$

(7) can be rewritten as

$$A_s(z) = \frac{A_s(\text{front})}{1 + 2.303\,c\,\dfrac{d\left[\log_{10} A_s(z)\right]}{dz}} \tag{10}$$

Since the correction of $A_{s(\text{front})}$ to $A_s(z)$ is not large (less than 10%) $\dfrac{d\left[\log_{10} A_s(\text{front})\right]}{dz}$ can be substituted for $\dfrac{d\left[\log_{10} A_s(z)\right]}{dz}$ in equation (10) with negligible error and

$$A_s(z) = \frac{A_s(\text{front})}{\left(1 + 2.303 \times 0.950\,\dfrac{d\left[\log_{10} A_s(\text{front})\right]}{dz}\right)} \tag{11}$$

$$= \frac{A_s(\text{front})}{\left(1 + 2.187\,\dfrac{d\left[\log_{10} A_s(\text{front})\right]}{dz}\right)}.$$

Table VI gives the values of $\dfrac{d\left[\log_{10} A_s(\text{front})\right]}{dz}$ and the true values of $\dfrac{d\left[\log_{10} A_s(\text{front})\right]}{dz}$ were obtained by numerical differentiation of the data of Table V which were then fitted to a smooth curve and values read from the curve at the z values given. It will be noted that the maximum correction at any point is about 9%, with no correction at the origin and a constant percent correction from 100 to 120 cm. The corrected distributions are shown as the lower curves in Fig. 3.

(H) Calculation of the Moments $\overline{z^{2n}}$

Table VII gives the values of $A_s\,z^4$ -- $A_s z^{12}$, calculated from the data of Table VI. Table VIII gives the values of $\int_0^{120} A_s\,z^{2n}\,dz$ obtained.

TABLE VI

THE DERIVATIVE OF LOGARITHM OF SATURATED ACTIVITY (FRONT) WITH RESPECT TO dz: SATURATED ACTIVITY AND LOGARITHM OF SATURATED ACTIVITY WITH TRANSPORT CORRECTIONS, $A_s(t)$

z in cm.	$\frac{d\left[\log_{10} A_s(\text{front})\right]}{dz}$	$A_s(t)$	$\text{Log}_{10} A_s(t)$
0	.00000	1.035×10^6	6.0149
2	.00200	1.022×10^6	6.0096
4	.00371	1.006×10^6	6.0026
6	.00543	9.770×10^5	5.9899
8	.00714	9.490 "	5.9773
10	.00880	9.115	5.9598
12	.01049	8.713	5.9402
14	.01215	8.216	5.9147
16	.01385	7.745	5.8890
18	.01553	7.170	5.8555
20	.01720	6.637	5.8220
22	.01880	6.061	5.7825
24	.02040	5.483	5.7390
26	.02190	4.951	5.6946
28	.02352	4.428	5.6462
30	.02500	3.953	5.5969
32	.02635	3.497	5.5437
34	.02764	3.094×10^5	5.4905

TABLE VI (cont'd.)

z in cm.	$\frac{d\left[\log_{10} A_s \text{ front}\right]}{dz}$	$A_s(t)$	$\text{Log}_{10} A_s(t)$
36	.02885	2.701×10^5	5.4315
38	.03003	2.380 "	5.3766
40	.03112	2.067	5.3153
42	.03215	1.781	5.2507
44	.03312	1.534	5.1858
46	.03405	1.309	5.1169
48	.03495	1.112	5.0461
50	.03575	9.451×10^4	4.9755
52	.03665	7.971 "	4.9015
54	.03729	6.761	4.8300
56	.03805	5.641	4.7514
58	.03880	4.728	4.6747
60	.03955	3.963	4.5980
62	.04030	3.299	4.5184
64	.04105	2.746	4.4387
66	.04181	2.276	4.3572
68	.04256	1.885	4.2753
70	.04332	1.558	4.1926
72	.04396	1.283	4.1082
74	.04445	1.047	4.0200
76	.04479	8.500×10^3	3.9294
78	.04498	6.907×10^3	3.8393

[redacted]

TABLE VI (cont'd.)

z in cm.	$\frac{d\,[\log_{10} A_s \text{ front}]}{dz}$	$A_s(t)$	$\text{Log}_{10} A_s(t)$
80	.04500	5.614×10^3	3.7493
82	.04488	4.564 "	3.6594
84	.04458	3.712	3.5696
86	.04406	3.021	3.4802
88	.04325	2.482	3.3948
90	.04175	2.042	3.3101
92	.04036	1.692	3.2284
94	.03965	1.409	3.1489
96	.03954	1.175×10^3	3.0700
98	.03954	9.821×10^2	2.9922
100	.03954	8.204 "	2.9140
102	.03954	6.887	2.8380
104	.03954	5.742	2.7591
106	.03954	4.775	2.6790
108	.03594	3.982	2.6001
110	.03954	3.312	2.5201
112	.03954	2.767	2.4420
114	.03954	2.302	2.3621
116	.03954	1.919	2.2831
118	.03954	1.600	2.2041
120	.03954	1.331×10^2	2.1242

[redacted]

TABLE VII

VALUES OF $A_z z^{2n}$ VERSUS z CALCULATED FROM VI

z	$A_s z^2$	$A_s z^4$	$A_s z^6$	$A_s z^8$	$a_s z^{10}$	$A z^{12}$
0	0	0	0	0	0	0
2	4088×10^7	$.01635 \times 10^9$	$.00000654 \times 10^{13}$	$.2616 \times 10^9$	$.0001046 \times 10^{13}$	$.0004184 \times 10^{13}$
4	1.610×10^7	$.2576 \times 10^9$	$.0004122 \times 10^{13}$	$.006595 \times 10^{13}$	$.1055 \times 10^{13}$	$.0001688 \times 10^{17}$
6	3.517 "	1.266×10^9	$.004558 \times 10^{13}$	$.1641 \times 10^{13}$	$.0005908 \times 10^{17}$	$.02127 \times 10^{17}$
8	6.074	3.887 "	.02488 "	1.592×10^{13}	$.01019 \times 10^{17}$	$.0006522 \times 10^{20}$
10	9.115	9.115	.09115	9.115×10^{13}	$.09115 \times 10^{17}$	$.0009115 \times 10^{20}$
12	12.55	18.07	.2602	$.003747 \times 10^{17}$	$.5396 \times 10^{17}$	$.07770 \times 10^{20}$
14	16.10	31.56	.6186	.01212 "	$.002376 \times 10^{20}$	$.4657 \times 10^{20}$
16	19.83	50.76	1.299	.03325	.008512	$.0002179 \times 10^{24}$
18	23.23	72.27	2.439	.07902	.02560	.0008294 "
20	26.55	106.2	4.248	.1699	.06796	.002718
22	29.34	142.0	6.873	.3327	.1610	.007792
24	31.58	181.9	10.48	.6036	.3477	.02003
26	33.47	226.3	15.30	1.034	.6990	.04725
28	34.72	272.2	21.34	1.673	1.312	.1029
30	35.58	320.2	28.82	2.594	2.335	.2102
32	35.81	366.7	37.55	3.845	3.937	.4031
34	35.77	413.5	47.80	5.526	6.388	.7385
36	35.00	453.6	58.79	7.619	9.874	1.280
38	34.37	496.3	71.67	10.35	14.95	2.159
40	33.07×10^7	529×10^9	84.66×10^{13}	13.55×10^{17}	21.68×10^{20}	3.469×10^{24}

TABLE VII (cont'd.)

cm. z	$A_s z^2$	$A_s z^4$	$A_s z^6$	$A_s z^8$	$A_s z^{10}$	$A_s z^{12}$
42	31.42×10^7	554.2×10^9	97.76×10^{13}	17.24×10^{17}	30.41×10^{20}	5.364×10^{24}
44	29.70 "	576.3 "	111.6 "	21.61 "	41.84 "	8.100 "
46	27.70	586.1	124.0	26.24	55.52	11.75
48	25.62	590.3	136.0	31.33	72.18	16.63
50	23.63	590.8	147.7	36.93	92.33	23.08
52	21.55	582.7	157.6	42.62	115.2	31.15
54	19.22	575.0	167.7	48.90	142.6	41.58
56	17.69	554.8	174.0	54.57	171.1	53.66
58	15.90	534.9	179.9	60.52	203.6	68.49
60	14.27	513.7	184.9	66.56	239.6	86.26
62	12.68	487.4	187.4	72.04	276.9	106.4
64	11.25	460.8	188.7	77.29	316.6	129.7
66	9.914	431.9	188.1	81.94	356.9	155.5
68	8.829	408.3	188.8	87.30	403.7	186.7
70	7.634	374.1	183.3	89.82	440.1	215.6
72	6.651	344.8	178.7	92.64	480.2	248.9
74	5.733	313.9	171.9	94.13	515.5	282.3
76	4.910	283.6	163.8	94.61	546.5	315.7
78	4.202	255.6	155.5	94.61	575.6	350.2
80	3.593	230.0	147.2	94.61	602.9	385.9
82	3.069	206.4	138.8	93.33	627.6	422.0
84	2.619×10^7	184.8×10^9	130.4×10^{13}	92.01×10^{17}	649.2×10^{20}	458.1×10^{24}

TABLE VII (cont'd.)

cm. z	$A_s z^2$	$A_s z^4$	$A_s z^6$	$A_s z^8$	$A_s z^{10}$	$A_s z^{12}$
86	2.234×10^7	165.2×10^9	122.2×10^{13}	90.38×10^{17}	668.5×10^{20}	494.4×10^{24}
88	1.922 "	148.8 "	115.2	89.21 "	690.8 "	535.0 "
90	1.654	134.0	108.5	87.89	711.9	576.6
92	1.432	121.2	102.6	86.84	735.0	622.1
94	1.245	110.0	97.20	85.89	758.9	670.6
96	1.083	99.81	91.98	84.77	781.2	720.0
98	.9432	90.58	86.99	83.55	802.4	770.6
100	.8204	82.04	82.04	82.04	820.4	820.4
102	.7165	74.54	77.55	80.68	839.4	873.3
104	.6211	67.18	72.66	78.59	850.0	919.4
106	.5365	60.28	67.73	76.10	855.1	960.8
108	.4645	54.18	63.20	73.72	859.9	1003
110	.4008	48.50	58.69	71.01	859.2	1040
112	.3471	43.54	54.62	68.52	859.6	1078
114	.2992	38.88	50.53	65.67	853.4	1109
116	.2582	34.74	46.75	62.91	846.5	1139
118	.2228	31.02	43.19	60.14	837.4	1166
120	$.1917 \times 10^7$	27.60×10^9	39.74×10^{13}	57.23×10^{17}	824.1×10^{20}	1187×10^{24}

TABLE VIII

THE z^{2n} MOMENTS

n	$\int_0^{120} A_s z^{2n} dz$	$k\int_{120}^{\infty} -E_i(-\frac{z}{\lambda}) z^{2n} dz$	$\frac{k\int_{120}^{\infty} -E_i(-\frac{z}{\lambda}) z^{2n} dz}{\int_0^{120} A_s z^{2n} dz + k\int_{120}^{\infty} -E_i(\frac{z}{\lambda}) z^{2n} dz}$	$\overline{z^{2n}}$
0	2.8472×10^{7}	1.5020×10^{3}	5.275×10^{-5}	
1	1.5628×10^{10}	2.5953×10^{7}	1.658×10^{-3}	5.4976×10^{2}
2	2.9516×10^{13}	4.6538×10^{11}	1.552×10^{-2}	1.0529×10^{6}
3	1.0515×10^{17}	8.7382×10^{15}	7.672×10^{-2}	3.9998×10^{9}
4	5.7487×10^{20}	1.7461×10^{20}	2.330×10^{-1}	2.6322×10^{13}
5	4.2118×10^{24}	3.7996×10^{24}	4.743×10^{-1}	2.8136×10^{17}
6	3.7402×10^{28}	9.2745×10^{28}	7.126×10^{-1}	4.5708×10^{21}

(H) Calculation of the Moments $\overline{z^{2n}}$

Table VII gives the values of $A_s z^2$, $A_s z^4$ -- $A_s z^{12}$, calculated from the data of Table VI. Table VIII gives the values of $\int_0^{120} A_s z^{2n} dz$ obtained by numerical integration, the values of $k\int_{120}^{\infty} -E_i(-z/\lambda) z^{2n} dz$ and the percentage of total integrals $\int_0^{\infty} A_s z^{2n} dz$, which were obtained from the extrapolated portions.

The value of k used in the extrapolation of $A_s(z)$ from 120 cm. to ∞ was obtained by fitting a function $A_s = k\left[-E_i(-z/\lambda)\right]$ to join the experimental curve at $z = 120$ cm. and λ was chosen to be consistent with

the last few points of the measured part distribution. The values for these constants used were $k = 2.899 \times 10^7$ and $\lambda = 12.116$ cm.

Table VIII also gives the values of $\overline{z^{2n}}$, i.e. $\overline{z^2}$, $\overline{z^4}$ -- $\overline{z^{12}}$, obtained from equation (2).

(I) Corrections for the Finite Size of the Graphite Sample and the $\cos\frac{\pi x}{a}\cos\frac{\pi y}{a}$ Source

The $\overline{\tau^n}$ Moments.

As pointed out in the introduction, the theoretical treatment of Weinberg and Rose makes possible the calculation, from the $\overline{z^{2n}}$ moments measured in the finite block with a plane $\cos\frac{\pi x}{a}\cos\frac{\pi y}{a}$ source, to the moments for a point source in an infinite medium.

Briefly, the corrections are made as follows: If $f(\tau)$ represents the primary energy distribution of the neutrons from the fission source normalized on a τ-scale, so that

$$\int_0^\infty f(\tau)\, d\tau = 1 \tag{12}$$

then the average age, $\overline{\tau}$, over the fission spectrum is defined as

$$\overline{\tau} = \int_0^\infty f(\tau)\, \tau\, d\tau \tag{13}$$

or in general, including the higher average moments, $\overline{\tau^n}$

$$\overline{\tau^n} = \int_0^\infty f(\tau)\, \tau^n\, d\tau \quad n = 1, 2 \text{ ---} \tag{14}$$

The treatment of Weinberg and Rose expresses the $\overline{\tau^n}$ in terms of the

measured $\overline{z^{2n}}$ moments and the geometry of the experiment by the following equation:

$$\overline{\tau^n} = \frac{\sum_{\nu=0}^{\infty} \frac{\Delta^{\nu}}{\nu!} \frac{(n+\nu)!}{(2n+2\nu)!} \overline{z^{(2n+2\nu)}}}{\sum_{\nu=0}^{\infty} \frac{\Delta^{\nu}}{2\nu!} \overline{z^{(2\nu)}}} \qquad (15)$$

where $\nu = 0, 1, 2 \ldots\ldots\ldots\ldots$, $\Delta = \frac{2\pi^2}{a^2}$ and, a, is determined experimentally by fitting $\cos \frac{\pi x}{a}$ to the measured transverse indium resonance distribution just above the source. In this experiment a = 129.3 cm. and $\Delta = 1.180\ \text{cm}^{-2}$ and the $\overline{z^{(2n+2\nu)}}$ and $\overline{z^{2\nu}}$ are the $\overline{z^2}$, $\overline{z^4}$, etc. as measured and listed in Table VIII. The value of $\overline{\tau}$ corresponds to $\frac{\overline{z^2}}{2}$ if $\overline{z^2}$ were measured in an infinite sample with an infinite uniform plane source or to $\frac{\overline{r^2}}{6}$ if $\overline{r^2}$ were measured in an infinite sample with a point source.

It should be emphasized that the derivation of formula (15) requires no assumptions about the nature of the fission spectrum nor does it assume any particular slowing down theory. It involves only geometrical transformations which make possible reduction of measurements made in a particular geometry to the more idealized point source, infinite medium geometry as described above.

Table IX gives the values of $\overline{\tau(\nu)}$, $\overline{\tau^2(\nu)}$ and $\overline{\tau^3(\nu)}$ calculated from (15) using the values of ν indicated and values of $\overline{z^{2n}}$ taken from Table VIII. Values of $\overline{\tau^n(\nu)}$ indicate how formula (15) converges for

increasing values of ν. It will be noted that $\overline{\tau}$ becomes constant, well within the experimental accuracy of the measured distribution, for values of $\nu \geq 3$ and $\overline{\tau^2}$ changes negligibly from $\nu = 3$ to $\nu = 4$. However, $\overline{\tau^3}$ is still changing, though very slowly, between $\nu = 2$ and $\nu = 3$. For this reason no $\overline{\tau^n}$ for $n > 3$ were calculated, since these would need values of $\overline{z^{2n}}$ with $n > 6$ and these would be very largely determined by the extrapolated portion of the slowing down distribution, from $z = 120$ cm. to $z = \infty$, which is almost certainly an underestimate as the λ in the, k $\left[-E_i\left(-\frac{z}{\lambda}\right)\right]$, extrapolating function, would continue to increase if one could measure the slowing down distribution for values of $z > 120$ cm.

(K) Corrections for Density of the Graphite

Since the density of our sample of graphite was 1.652 ± 0.003 g/cm^3 and it is customary to correct the age and higher $\overline{\tau^n}$ moments to a standard density of 1.600 g/cm^3, Table X gives $\overline{\tau}$, $\overline{\tau^2}$ and $\overline{\tau^3}$ before and after this correction has been made using the well known fact that $\overline{\tau} \propto \frac{1}{\rho^2}$, etc. Since the age varies inversely as ρ^2, it is important that the actual stacking density be accurately known for the sample. Consequently the density was measured when the column was unstacked by weighing 236 of the 360 stringers, determining the average density for stringer and then computing the weight of the 360 stringers. This was then divided by the volume of the stack from its measured

[redacted]

TABLE IX

VALUES OF $\overline{\tau^n}$ WITH AND WITHOUT TRANSPORT CORRECTION

	$\overline{\tau^n}$ Without Transport Correction			$\overline{\tau^n}$ With Transport Correction		
ν	1	2	3	1	2	3
0	283.1	9.200×10^4	3.516×10^7	274.9	8.774×10^4	3.333×10^7
1	293.6	10.01×10^4	4.095×10^7	285.7	9.595×10^4	3.913×10^7
2	297.6	10.37×10^4	4.394×10^7	289.9	9.959×10^4	4.208×10^7
3	298.8	10.49×10^4	4.502×10^7	291.1	10.08×10^4	4.316×10^7
4	299.1	10.52×10^4		291.3	10.11×10^4	
5	299.2			291.4		

TABLE X

FINIAL VALUES OF τ, $\overline{\tau^2}$, and $\overline{\tau^3}$ BEFORE AND AFTER CORRECTION TO GRAPHITE DENSITY OF 1.600 g/cm^3

	$\overline{\tau^n}$ Without Density Correction			$\overline{\tau^n}$ With Density Correction		
ν	1	2	3	1	2	3
0	274.9	8.774×10^4	3.333×10^7	293.0	9.967×10^4	4.036×10^7
1	285.7	9.595×10^4	3.913×10^7	304.6	10.90×10^4	4.739×10^7
2	289.9	9.959×10^4	4.208×10^7	309.0	11.31×10^4	5.096×10^7
3	291.1	10.08×10^4	4.316×10^7	310.3	11.45×10^4	5.227×10^7
4	291.3	10.11×10^4		310.6	11.48×10^4	
5	291.4			310.6		

[redacted]

dimensions, giving the true stacking density of the sample.

III. RESULTS AND CONCLUSIONS

(A) Comparison of this Determination of $\overline{\tau}$ with Previously Reported Work

The value of $\overline{\tau}$ 318.9 cm^2 obtained without transport corrections agrees with the value 317 cm^2, obtained by E. Fermi, J. Marshall and L. Marshall (CP-1084) very well (0.6%), if it is assumed that Fermi et al did not make the transport corrections described in 2-g. These authors make no statement as to whether or not transport corrections were made and it seems likely that they did not.

The value of $\overline{\tau}$ with transport corrections was 310.6 cm^2 or 2.6% less than the value without the transport correction.

A simple calculation, on the basis of Fermi age theory, gives a rough estimate of the magnitude of transport correction to be expected, and the result

$$\overline{\tau}\ (\text{uncorrected}) = \overline{\tau}\left(1 + \frac{2c}{\sqrt{\pi\,\overline{\tau}}}\right) \qquad (16)$$

where, c, is the constant defined in 2-g. Equation (16) predicts that the value of $\overline{\tau}$ with transport correction, should be approximately 3% less than the uncorrected value, in good agreement with the experimental difference of 2.6% given above.

(B) Limits of Error in $\overline{\tau}$ and Higher Moments

The limits of error to be assigned to $\overline{\tau^n}$ moments are difficult to estimate rigorously because of the contribution of the extrapolated portions of the $\overline{z^{2n}}$ moments and the rather involved manner in which each of the $\overline{\tau^n}$

are related to several of the $\overline{z^{2n}}$ through equation (16). However, in the case of $\overline{\tau}$, these more complicated factors contribute relatively little to the estimated uncertainty in the result, as will be shown in more detail below.

The factors which contribute to the uncertainty in the final value of $\overline{\tau}$ of 310.6 cm^2 are as follows:

(1) Experimental uncertainties in the measured portions of the $\overline{z^{2n}}$ moments.

(2) Experimental uncertainty in the density of the sample used to correct to a standard density of 1.600 g/cm^3.

(3) Experimental uncertainty in the transport corrections from uncertainties in the constant, c, and the values of $\frac{d\,A_{s(front)}}{dz}$.

(4) Uncertainties in the extrapolated portions of the $\overline{z^{2n}}$ due to the fact that the extrapolating function $k\left[-E_1\left(-\frac{z}{\lambda}\right)\right]$ is an underestimate of the portion of the distribution from $z = 120$ cm. to $z = \infty$, since λ increases slowly with z through the measured region of the distribution for $z < 120$ cm. However, for sufficiently large z, λ should approach a constant value since there is certainly a finite upper limit to the energy of fission neutrons and consequently λ will probably not increase greatly for large z.

Statistical analysis based on the total number of counts entering into the measurement of the original slowing down distribution indicate that the uncertainties in $\overline{z^{2n}}$ from source (1) are less than 0.3%.

[redacted]

The uncertainty in the density of the sample is 0.2%, which contributes an uncertainty to $\overline{\tau}$ at a density of 1.6 g/cm^3 from source (2) of 0.4%.

The experimental uncertainty in the transport correction at any given point of the distribution is not greater than $\pm$ 5%. Since the total contribution of the transport corrections to $\overline{\tau}$ was only 2.6%, this indicates that the uncertainty in $\overline{\tau}$ from source (3) is certainly less than 0.13%.

Equation (16), using enough $\overline{z^{2n}}$ moments to give a stationary value of $\overline{\tau}$, increases the first term in the expansion, $\frac{\overline{z^2}}{2}$, by only 5.7% and each additional term in the expansion contributes a rapidly decreasing part of this 5.7%. Thus, if all the extrapolated parts of the z^{2n} moments out to $\overline{z^{12}}$ were discarded the change in $\overline{\tau}$ is only 1.1%. Consequently, if the extrapolated portions of the $\overline{z^{2n}}$ moments were as much as 20% in error, the error in $\overline{\tau}$ due to source (4) would be only 0.2%, which is small compared with the other sources of error. It is concluded that the uncertainty in $\overline{\tau}$ = 310.6 cm^2 is surely not greater than 1%.

Similarly, the uncertainties in $\overline{\tau^2}$ and $\overline{\tau^3}$ are estimated to be less than 3% and 6% respectively.

In conclusion, it appears that this experimental method, using a finite sample and a $\cos\frac{\pi x}{a}\cos\frac{\pi y}{a}$ plane source, gives reliable results with a reasonable size sample. It has definite advantages over a point source experiment in that one can measure to greater distances from the source, no geometry corrections are necessary and all the measurements can be taken with one source and detecting foil size.

[redacted]

[redacted]

ACKNOWLEDGEMENTS

The authors wish to express appreciation to Dr. A. M. Weinberg, Dr. M. E. Rose and Dr. E. O. Wollan for their many helpful suggestions during the course of these investigations and thanks are also due T. E. Fitch for frequent help in counting foils and reducing of data.

[redacted]